Simulation study of the magnetized sheath of a dusty plasma

G. Foroutan, H. Mehdipour, and H. Zahed

Citation: Physics of Plasmas (1994-present) **16**, 103703 (2009); doi: 10.1063/1.3243497
View online: http://dx.doi.org/10.1063/1.3243497
View Table of Contents: http://scitation.aip.org/content/aip/journal/pop/16/10?ver=pdfcov
Published by the AIP Publishing

Simulation study of the magnetized sheath of a dusty plasma

G. Foroutan,[1,2] H. Mehdipour,[1] and H. Zahed[1]
[1]*Department of Physics, Faculty of Science, Sahand University of Technology, 51335-1996 Tabriz, Iran*
[2]*School of Physics, The University of Sydney, New South Wales 2006, Sydney, Australia*

(Received 30 July 2009; accepted 14 September 2009; published online 12 October 2009)

Numerical solutions of stationary multifluid equations are used to study the formation and properties of the magnetized sheath near the boundary of a dusty plasma. The impacts of the strength of the magnetic field, the dust and plasma number densities, and the electron temperature on the sheath structure and spatial distributions of various quantities are investigated. It is shown that for a given angle of incidence of the magnetic field, there is a threshold magnetic field intensity above which some kind of large regular inhomogeneities develop on the spatial profile of the dust particles. The sheath thickness, the electron and ion number densities, and the absolute dust charge are strongly affected by the variation in the dust number density. The sheath demonstrates a nonlinear dependence on the electron temperature; as the electron temperature rises, the sheath first is broadened and the absolute wall potential decreases but then at higher temperatures the sheath becomes narrower and the absolute wall potential increases. © *2009 American Institute of Physics*. [doi:10.1063/1.3243497]

I. INTRODUCTION

The problem of sheath formation at the boundary of a plasma is of fundamental importance in many applications including plasma probes, low-temperature plasma-aided material processing, as well as fusion research.[1–3] Due to the high mobility of the electrons, the wall potential remains negative with respect to the main body of the plasma. A negative potential barrier prevents further escape of the electrons and results in the formation of a positive space-charge sheath, a Debye sheath, shielding the neutral plasma from the negative wall. The typical sheath thickness is a few electron Debye length λ_D, which is usually small compared with the characteristic length of the plasma defined by the typical size of the system. For the electrostatic sheath formation the ions must enter the sheath region at least with ion sound velocity, the so-called Bohm criterion. Numerous publications can be found in the literature devoted to the study of the different properties of sheaths in unmagnetized two component plasmas.[4–12]

When an oblique magnetic field is applied to the plasma, then Chodura[13] stated that a magnetic presheath region arises upstream of the Debye sheath, where there is also a significant electric field. According to Chodura's model, plasma particles pass through three distinct regions on their way toward the wall. The first one, called plasma presheath, is the quasineutral plasma region where electrons are accelerated along magnetic field lines due to the electron pressure gradient. Therefore, an electric field is generated which in turn accelerates the ions along the magnetic field up to ion sound speed. The second region (the Chodura layer) is the quasineutral magnetized presheath where the electric field becomes strong enough to deflect the ions from their motion along the magnetic field lines. The ions enter the Chodura layer when their velocity component in the direction of the magnetic field reaches the ion sound speed (the Chodura criterion). The scale size of the magnetic presheath is the ion Larmor radius ρ_i. The third region, Debye sheath, is a region of net, positive space-charge density with strong electric field that directs the ions toward the wall. However, experiments[14] do not support Chodura's theory suggesting that the Chodura layer is a consequence of the particular mathematical modeling. It was shown in Refs. 15 and 16 that the Chodura layer can be eliminated if ion-neutral collisions are taken into account. For a detailed discussion of the effects of magnetic field on the sheath structure and the dynamics of electrons and ions we refer to Refs. 17–29.

A dusty plasma is simply defined as a multicomponent admixture of electrons, ions, and charged dust particles with size ranging from nanometers to micrometers. Dust particles are often observed to be localized in the plasma boundary near solid objects or walls, such as the planetary rings and comets, artificial satellites, in the devices for plasma assisted material and chemical processing, plasma discharges, as well as the wall region of hot fusion plasmas.[30–43] In processing discharges, dust particles can be created due to coagulation of various components with their subsequent transport into the sheath. The dust grain is charged by the collection of the plasma particles (electrons and ions) flowing onto its surface. Since the electron thermal speed is much larger than the ion thermal speed, the grain acquires much more electrons than ions, and as a result its surface potential becomes negative. The grains of a few micrometers in size have hundreds to thousands of elementary charges. In plasma processing reactors negatively charged dust particles appear as contamination to etching, sputtering, and deposition processes. Moreover, the growth of dust grain in discharges offers unique possibilities for powder synthesis and surface modification processes. The sheath containing negatively charged dust particles is, therefore, relevant to plasma-wall interaction in various plasma-aided industrial applications.

The problem of plasma-wall transition in the presence of charged dust particles has been investigated by several

authors.[44–60] Ma *et al.*[48] studied the electrostatic sheath of a one-dimensional dusty plasma assuming that the electrons are in thermal equilibrium and their density is given by the Boltzmann relation, while the ions and dust grains are considered as cold fluids. Among the force acting on the dust grains only the electrostatic and gravitational forces were taken into account. They found that for the small dust grains, for which gravity is negligible, the sheath potential exhibits a solitonlike profile and the dust density is strongly localized. But, when the two forces are comparable, a stratification of the dust density occurs and the electrostatic potential as well as the electron and ion densities show an oscillatory behavior. Resendes *et al.*[53] developed a theoretical model to explain the large amplitude self-excited dust particle oscillations in the plasma sheath. The dynamics of a dust particle in magnetized plasma sheath has recently been investigated using a two-fluid model.[57–59] The main effect of an oblique magnetic field on the sheath characteristics is to induce oscillations in the spatial variation of the ion's velocity and density. The sheath thickness decreases with increasing the strength of the magnetic field and its angle of incidence with normal to the wall.

So far, the study of magnetized plasma sheath in the presence of dust particles has been restricted to a single dust particle. To the best of our knowledge there is no report on the collective behavior of dust particles in a magnetized plasma sheath, or in other words, in a magnetized dusty plasma sheath. However, due to their macroscopic size, the charge number of the dust particles can be very large and, if they are numerous in the sheath, can produce strong electric fields. So, their role in determination of the overall characteristics of the sheath, such as the sheath potential, cannot be neglected and a self-consistent description of dusty plasma sheath should include the charge of the dust particles in the space charge. In this work, we investigate the structure of a dusty plasma sheath in the presence of an oblique magnetic field. A multifluid model is used to simulate the dynamics of the electrons, ions, and dust particles. Our model equations include the effects of the electric, magnetic, and gravitational forces. The orbit motion limited (OML) theory of the grain charging is employed to calculate the charge on the dust particles. For a self-consistent evaluation of the sheath potential, the charges of the dust particles are included in the Poisson equation. The dependence of the electron, ion, and dust densities, their normal velocities, as well as the sheath potential and the dust charge on the applied magnetic field, dust properties, and the bulk plasma parameters is investigated.

This paper is organized as follows. In Sec. II we introduce the sheath model and set up the basic equations to be solved numerically. The results of the numerical simulations for the sheath structure and the density and velocity distributions of the particles are presented and discussed in Sec. III. Finally, the main findings are summarized and enumerated in Sec. IV.

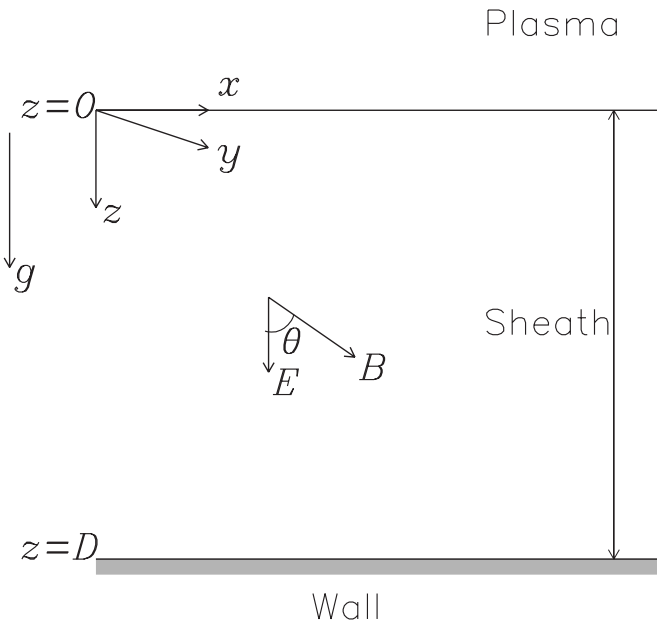

FIG. 1. The geometry of the magnetized plasma sheath.

II. MODEL AND BASIC EQUATIONS

We consider the wall region of a magnetized stationary ($\partial_t=0$) dusty plasma. The magnetic field, which is spatially uniform and constant in time, lies in the (x,z) plane and makes an angle θ with the z axis. The geometry of the simulation region is presented in Fig. 1. The plasma-sheath boundary is located at $z=0$ with the plasma filling the half space $z<0$. The plasma-wall transition layer is considered as a unit without splitting it into the presheath and sheath sublayers. It is assumed that the sheath is infinitely long in x and y directions while the physical properties change only in the z (normal to the wall) direction.

The standard fluid model is used to investigate the dynamics of the plasma and dust particles in the sheath region. The neutral particles are assumed to be immobile and uniformly distributed throughout the plasma sheath. In the equations for the electrons and ions, we include the effects of ionization and collisions with neutrals, but electron-ion collisions are neglected. For the dust particles, the electric, magnetic, and gravitational forces are assumed as the dominant forces but the effects of ion drag, neutral drag, and thermophoretc forces are ignored. The interaction between the dust grains is also disregarded. The governing equations are the continuities

$$\frac{d}{dz}(n_d v_{dz}) = 0, \tag{1}$$

$$\frac{d}{dz}(n_i v_{iz}) = \gamma_{\text{ion}} n_n n_e, \tag{2}$$

$$\frac{d}{dz}(n_e v_{ez}) = \gamma_{\text{ion}} n_n n_e, \tag{3}$$

and momentum equations

$$m_d v_{dz}\frac{dv_{dx}}{dz} = \frac{q_d}{c}Bv_{dy}\cos\theta, \tag{4}$$

$$m_d v_{dz}\frac{dv_{dy}}{dz} = \frac{q_d}{c}B(v_{dz}\sin\theta - v_{dx}\cos\theta), \tag{5}$$

$$m_d v_{dz}\frac{dv_{dz}}{dz} = -q_d\left(\frac{d\phi}{dz} + \frac{1}{c}Bv_{dy}\sin\theta\right) + m_d g, \tag{6}$$

$$m_i v_{iz}\frac{dv_{ix}}{dz} = \frac{e}{c}Bv_{iy}\cos\theta - m_i\nu_{in}v_{ix}, \tag{7}$$

$$m_i v_{iz}\frac{dv_{iy}}{dz} = \frac{e}{c}B(v_{iz}\sin\theta - v_{ix}\cos\theta) - m_i\nu_{in}v_{iy}, \tag{8}$$

$$m_i v_{iz}\frac{dv_{iz}}{dz} = -e\left(\frac{d\phi}{dz} + \frac{1}{c}Bv_{iy}\sin\theta\right) - \frac{T_i}{n_i}\frac{dn_i}{dz} - m_i\nu_{in}v_{iz}, \tag{9}$$

$$0 = -\frac{e}{c}Bv_{ey}\cos\theta - m_e\nu_{en}v_{ex}, \tag{10}$$

$$0 = -\frac{e}{c}B(v_{ez}\sin\theta - v_{ex}\cos\theta) - m_e\nu_{en}v_{ey}, \tag{11}$$

$$0 = e\left(\frac{d\phi}{dz} + \frac{1}{c}Bv_{ey}\sin\theta\right) - \frac{T_e}{n_e}\frac{dn_e}{dz} - m_e\nu_{en}v_{ez} \tag{12}$$

for the dust grains, ions, and electrons, where the electron inertia has been neglected. In the above equations, m_j is the mass, n_j is the number density, v_{jx}, v_{jy}, and v_{jz} are the x, y, and z components of the fluid velocities of particle species j, and ϕ, q_d, γ_{ion}, and ν_{jn} are the sheath electric potential, the charge of the dust particles, the ionization rate, and the collision frequency with neutrals, respectively. We assume that the ion temperature T_i and the electron temperature T_e are constant. The electric potential is obtained from the Poisson equation,

$$\frac{d^2\phi}{dz^2} = 4\pi[e(n_e - n_i) - n_d q_d]. \tag{13}$$

The unperturbed plasma at $z=0$ satisfies the quasineutrality condition,

$$e(n_{i0} - n_{e0}) + n_{d0}q_{d0} = 0, \tag{14}$$

where n_{j0} is the unperturbed number density of species j at $z=0$.

The dust charge q_d is determined by the local microscopic electron and ion currents I_e and I_i flowing onto the grains. For micrometer-sized dust particles considered in this work, the characteristic time for the dust motion is of the order of 10^{-2} s,[61] while the dust charging time, i.e., the time for the dust to be charged from zero to the floating potential is estimated to be of the order of 10^{-5} s.[62] Therefore, the dust charging time is much smaller than the characteristic time for the dust motion, during the charging process the displacement of the grain is negligible, and the charging can be considered as a local phenomenon. Then the grain charge is determined by the balance of the electron and ion currents,

$$I_e + I_i = 0. \tag{15}$$

Spherical dust particles with radius r_d are considered in this work. The OML theory can be used to calculate the charging currents if $r_d \ll \lambda_{\text{De}} \ll \lambda_{\text{mfp}}$, where $\lambda_{\text{De}} = \sqrt{T_e/4\pi n_{e0}e^2}$ is the electron Debye length and λ_{mfp} is the neutral collision mean free path. Furthermore, in the presence of a magnetic field B, r_d must be smaller than the electron gyroradius, $\rho_e = \sqrt{T_e m_e c^2/e^2B^2}$. This condition can be satisfied if the magnetic field B is smaller than a critical value B_{cr} determined by[63]

$$B_{\text{cr}}\ (\text{kG})r_d\ (\mu\text{m}) = 41.37\sqrt{\frac{T_e\ (\text{eV})}{3\ (\text{eV})}}. \tag{16}$$

According to the OML theory the electron and ion currents to the dust particles are determined by local electron and ion densities, as well as the potential difference between the particle surface and the local plasma. Depending on the sign of the dust charge, these currents are given by[37,52,53]

$$I_e = -\pi r_d^2 e\left(\frac{8T_e}{\pi m_e}\right)^{(1/2)} n_e \exp\left(\frac{eq_d}{r_d T_e}\right), \tag{17}$$

$$I_i = \pi r_d^2 e n_i v_i\left(1 - \frac{2eq_d}{r_d m_i v_i^2}\right) \tag{18}$$

for $q_d < 0$ and

$$I_e = -\pi r_d^2 e\left(\frac{8T_e}{\pi m_e}\right)^{(1/2)} n_e\left(1 + \frac{eq_d}{r_d T_e}\right), \tag{19}$$

$$I_i = \pi r_d^2 e n_i v_i \exp\left(\frac{2eq_d}{r_d m_i v_i^2}\right) \tag{20}$$

for $q_d > 0$. To use these equations in the sheath situation, where we have a directed flow of ions toward the wall, the ion velocity in Eqs. (18) and (20) is replaced with the mean speed of ions approaching the dust particles.[64] The ion mean speed is obtained from

$$v_s = \left(\frac{8T_i}{\pi m_i} + \tilde{v}_i^2\right)^{1/2}, \tag{21}$$

where $\tilde{v}_i = v_i - v_d$ is the directed ion speed relative to a dust particle moving with velocity v_d. For a conducting dust grain, the particle charge is proportional to its potential relative to the surrounding plasma and is given by $q_d = r_d(\phi_d - \phi)$. By using this expression together with Eqs. (17)–(20) in Eq. (15), the normalized dust charge $Q(z,v_d) = e(\phi_d - \phi)/T_e$ can be calculated from

$$\left(\frac{T_e m_i}{T_i m_e}\right)^{1/2}\frac{n_e}{n_i}\exp(Q) = \tilde{v}_s\left[1 - \frac{T_e}{T_i}\frac{\pi Q}{4\tilde{v}_s^2}\right] \tag{22}$$

for $Q < 0$ and

$$\left(\frac{T_e m_i}{T_i m_e}\right)^{1/2} \frac{n_e}{n_i}(1+Q) = \tilde{v}_s \exp\left[-\frac{T_e}{T_i}\frac{\pi Q}{4\tilde{v}_s^2}\right] \tag{23}$$

for $Q \geq 0$, where $\tilde{v}_s = (1+\tilde{v}_i^2/v_{\text{thi}}^2)^{1/2}$ and $v_{\text{thi}} = \sqrt{8T_i/\pi m_i}$ is the ion mean thermal speed.

Equations (1)–(14) together with Eqs. (22) and (23) constitute a basic set of equations to investigate the dynamics of a magnetized plasma sheath in the presence of mobile dust particles. These equations do not contain the effects of the ion and neutral drag forces on the dust particles, the interactions between neighboring grains, and plasma-dust collisions for the electrons and ions. The ion and neutral drag forces are proportional to the square of the dust radius as well as the ion and neutral fluxes. Therefore, for large dust particles and high plasma densities the drag forces, specially the ion drag, could be large and comparable with the other forces in the sheath. But, with the plasma density and dust particle radius considered here, it can be shown that the electric, magnetic, and gravitational forces are the dominant forces. On the other hand, since the drag forces inside the sheath are always along the z direction, they are expected to enhance or reduce the effect of gravity. As the continuous fluid model is used to describe the dust dynamics, this requires the intergrain distance to be smaller than the electron Debye length. Moreover, for validity of OML theory the intergrain distance should be larger than the ion Debye length.[48] Therefore, with $n_{e0} \approx n_{i0} = 10^9$ cm^{-3}, $T_e = 1$ eV, and $T_i = 0.05$ eV, we are restricted to dust densities $1.2\times 10^5 < n_d < 7.1\times 10^6$ (in cm^{-3}). Our assumption of negligible dust-dust interactions is justified in this density range, but at higher dust densities one should take the dust correlation effects into account. To explain the reason for the neglect of dust-plasma interactions, it is noted that electron-dust and ion-dust collision frequencies are directly proportional to dust number density.[65] With the above dust density range, and as we consider a weakly ionized plasma with fractional ionization $n_{e0}/n_n \simeq 10^{-6}$, it can be shown that the frequency of neutral-plasma collisions is much larger than that of dust-plasma collisions. So, in the present work the neutral-plasma collisions are assumed to be the most important momentum transfer collisions, but at higher dust densities and degrees of ionization the effect of dust-plasma interactions could be significant and cannot be neglected.

For numerical simulation, Eqs. (1)–(14) are converted into dimensionless form using the following set of normalized variables:

$$\Phi = e\phi/T_e, \quad Q = eq_d/r_d T_e, \quad \xi = z/\lambda_{De},$$

$$N_j = n_j/n_{j0}, \quad \mathbf{u}_{i,e} = \mathbf{v}_{i,e}/c_{si}, \quad \mathbf{u}_d = \mathbf{v}_d/c_{sd}, \tag{24}$$

$$\bar{\nu}_{\text{ion}} = \nu_{\text{ion}}/\omega_{pi}, \quad \bar{\nu}_{in} = \nu_{in}/\omega_{pi}, \quad \bar{\nu}_{en} = m_e\nu_{en}/m_i\omega_{pi},$$

where $c_{si} = \sqrt{T_e/m_i}$ and $c_{sd} = \sqrt{ZT_e/m_d}$ are the ion-acoustic and dust-acoustic speeds and $\nu_{\text{ion}} = n_n\gamma_{\text{ion}}$ and $\omega_{pi} = \sqrt{4\pi n_{i0}e^2/m_i}$ are the ionization and ion plasma frequencies, respectively. The parameter $Z = r_d T_e/e^2$ is the dust charge number at $Q=1$, i.e., when the floating potential on the grain surface is T_e/e. Henceforth, we omit the bars over dimensionless frequencies since no confusion should result. Using the above normalization, the following set of coupled differential equations can be obtained from Eqs. (1)–(14):

$$\frac{dN_d}{d\xi} = Q\frac{N_d}{u_{dz}^2}\left(\frac{d\Phi}{d\xi} + \delta\beta_d u_{dy}\sin\theta\right) - \mu\frac{N_d}{u_{dz}^2}, \tag{25}$$

$$\frac{du_{dx}}{d\xi} = Q\delta\beta_d\frac{u_{dy}}{u_{dz}}\cos\theta, \tag{26}$$

$$\frac{du_{dy}}{d\xi} = Q\delta\beta_d\left(\sin\theta - \frac{u_{dx}}{u_{dz}}\cos\theta\right), \tag{27}$$

$$\frac{du_{dz}}{d\xi} = -\frac{Q}{u_{dz}}\left(\frac{d\Phi}{d\xi} + \delta\beta_d u_{dy}\sin\theta\right) + \frac{\mu}{u_{dz}}, \tag{28}$$

$$\frac{dN_i}{d\xi} = -\frac{N_i T_e}{T_i - u_{iz}^2 T_e}\left(\frac{d\Phi}{d\xi} + \delta\beta_i u_{iy}\sin\theta + \delta\nu_{in}u_{iz} + \delta^{-1}\nu_{\text{ion}}u_{iz}\frac{N_e}{N_i}\right), \tag{29}$$

$$\frac{du_{ix}}{d\xi} = \frac{\delta}{u_{iz}}(\beta_i u_{iy}\sin\theta - \nu_{in}u_{ix}), \tag{30}$$

$$\frac{du_{iy}}{d\xi} = \frac{\delta}{u_{iz}}[\beta_i(u_{iz}\sin\theta - u_{ix}\cos\theta) - \nu_{in}u_{iy}], \tag{31}$$

$$\frac{du_{iz}}{d\xi} = -\frac{1}{u_{iz}}\left(1 - \frac{T_i}{T_i - u_{iz}^2 T_e}\right)\left[\frac{d\Phi}{d\xi} + \delta\beta_i u_{iy}\sin\theta + \delta\nu_{in}u_{iz}\right] + \delta^{-1}\nu_{\text{ion}}\frac{N_e}{N_i}\frac{T_i}{T_i - u_{iz}^2 T_e}, \tag{32}$$

$$\frac{dN_e}{d\xi} = N_e\frac{d\Phi}{d\xi} - N_e\delta\nu_{en}u_{ez}\left[1 + \frac{\sin^2\theta}{\cos^2\theta + (m_i\nu_{en}/m_e\beta_i)^2}\right], \tag{33}$$

$$\frac{du_{ez}}{d\xi} = -u_{ez}\frac{d\Phi}{d\xi} + \delta\nu_{en}u_{ez}^2\left[1 + \frac{\sin^2\theta}{\cos^2\theta + (m_i\nu_{en}/m_e\beta_i)^2}\right] + \delta\nu_{\text{ion}}, \tag{34}$$

$$\frac{d^2\Phi}{d\xi^2} = N_e - \delta^2 N_i - (1-\delta^2)N_d\frac{Q}{Q_0}, \tag{35}$$

where $\delta = (n_{i0}/n_{e0})^{1/2}$, $\mu = g\lambda_{De}/c_{sd}^2$, $\beta_d = (Zm_i/m_d)^{1/2}\beta_i$, and $\beta_{i,e} = \omega_{ci,e}/\omega_{pi}$. The cyclotron frequency is given by $\omega_{cj} = |e|B/m_j c$ and the x and y components of the electron velocity can be expressed in terms of its z component as follows:

$$u_{ex} = \frac{\sin\theta\cos\theta}{\cos^2\theta + (m_i\nu_{en}/m_e\beta_i)^2}u_{ez}, \tag{36}$$

$$u_{ey} = -\frac{(m_i\nu_{en}/m_e\beta_i)\sin\theta}{\cos^2\theta + (m_i\nu_{en}/m_e\beta_i)^2}u_{ez}. \tag{37}$$

We specify the following boundary conditions at the sheath edge:

$$u_{d\perp} = u_{i\perp} = u_{ez} = 0, \quad u_{iz} = 1.3, \quad u_{dz} = 1.5,$$
$$N_d = N_i = N_e = 1, \quad \Phi = 0, \quad d\Phi/d\xi = \nu_{in}. \tag{38}$$

A small nonzero electric field is assumed at the sheath edge. This value is necessary for the smooth transition of the sheath solutions to the plasma solutions and to avoid the singularity at the sheath edge. According to the Bohm criterion the ion velocity at the sheath edge should be larger than ion sound speed. So, there must be a residual finite electric field in the bulk plasma to accelerate the ions to such velocities. For the collisionless case the sheath edge will formally be at infinity where the electric field is zero. But in reality the sheath edge will be at finite distance from the wall, and the electric field there will have a small finite value.[47]

Equations (25)–(35) with boundary conditions (38) are solved using a fourth-order Runge–Kutta method. Simultaneously, Eqs. (22) and (23) are solved to obtain the dust charge at every position self-consistently.

III. RESULTS OF NUMERICAL SIMULATIONS

In this section we present the numerical results for the structure of the dusty plasma sheath, obtained from computer simulations of the multifluid model described in Sec. II. Argon is considered to be the background gas with the following parameters as default parameters: $T_e=1$ eV, $T_i=0.05$ eV, $n_{e0}=10^9$ cm^{-3}, $\delta^2=1.9$, $\nu_{\text{ion}}=0.01$, $\nu_{in}=0.01$, and $\nu_{en}=0.002$. Other default parameters are $B=19$ kG, $\theta=20°$, $r_d=10^{-4}$ cm, and $\rho_d=3.5$ g cm^{-3}, where ρ_d is the mass density of a dust particle. The sheath thickness is determined by the requirement that the wall is located at the position of zero electron density. So the wall potential is not a constant and depending on the sheath dynamics can take different values.

Before presenting the results of the numerical simulations, it would be worth to examine the applicability of the OML theory. With the above mentioned parameters we have $\lambda_{\text{De}} \simeq 2\times 10^{-2}$ cm. On the other hand, for $n_n \simeq 10^{15}$ cm^{-3}, the ion mean free path is $\lambda_{\text{mfp}}=1/n_n\sigma \simeq 1$ cm.[59] Therefore, our default parameters satisfy the condition $r_d \ll \lambda_{\text{De}} \ll \lambda_{\text{mfp}}$ for validity of the OML theory. Furthermore, substituting the default parameters in Eq. (16) results in $B_{\text{cr}} \simeq 24$ kG which is well above the default value of 19 kG.

A. Effects of the magnetic field

Figure 2 shows the profiles of the sheath potential, the dust charge, the particle densities, and the particle normal velocities as functions of ξ for three different values of the magnetic field intensity. The Debye shielding and sheath formation are obvious from the distributions of the electrostatic potential and the ion and electron number densities. In the absence of the magnetic field, the most prominent feature of the dusty plasma sheath is the appearance of a layered structure in the spatial distribution of the dust grains as seen from the dashed N_d and u_{dz} curves in Fig. 2. This stratification of the dust particles is a result of balance between the electrostatic and gravitational forces.[48] Accordingly, small amplitude fluctuations develop on the distributions of the other sheath parameters, specially on the ion velocity and ion number density.

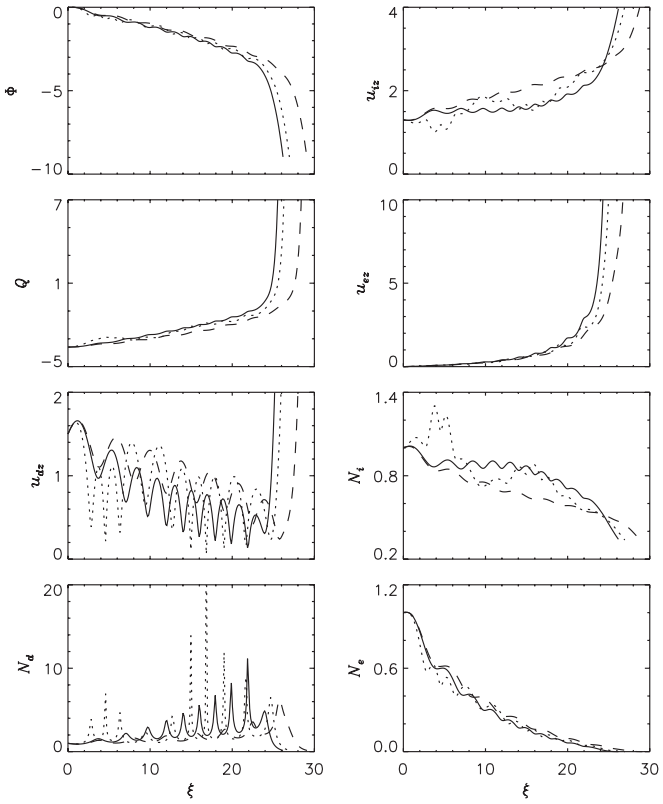

FIG. 2. Profiles of the sheath potential, the dust charge, the particle densities, and the particle velocities as functions of ξ for three different values of the magnetic field intensity: $B=0$ (dashed curves), 7.5 kG (solid curves), and 23.7 kG (dotted curves). The angle of the magnetic field with respect to the normal to the wall is 28° and all the other parameters are set to their default values.

When a moderate magnetic field with $B=7.5$ kG is applied, the sheath width decreases while the absolute value of the wall potential increases slightly. The ion normal velocity decreases in most parts of the sheath region except near the wall where it rises above that of $B=0$. The ion density acts reversely and increases up to close to the wall and then declines quickly. Compared with the ions, electrons are weakly affected by the magnetic filed. They experience an enhancement in their normal velocity near the wall and a slight reduction in their number density away from the sheath edge. The absolute dust charge and the mean dust normal velocity are reduced by the magnetic field but the level of stratification in the dust number density and dust normal velocity is increased. To explain the results mentioned above, we scrutinize the effect of the magnetic field on the densities and velocities of the particles through Eqs. (25)–(34). It is obvious from Eq. (32) that the magnetic field decelerates the ions as long as u_{iy} is positive and accelerate them when it changes sign. The numerical results showed us that u_{iy} assumes positive values from the sheath edge up to close to the wall and then becomes negative. Therefore, away from the wall the ion normal velocity decreases and consequently the ion density increases, but the reverse is happening near the wall. For

inertialess electrons, as seen from Eq. (34) the magnetic force is always in the z direction so their normal velocity increases and their number density decreases. Because of the reduction in the electron density and increasing the ion density, the absolute dust charge decreases. We found from the numerical results that u_{dy} is negative in the whole sheath region, so Eq. (28) indicates that the magnetic force on the dust particles is in the same direction as the electric force and decelerates their motion to the wall. This leads to enhancement of the level of stratification by increasing the number of dust density layers and their amplitudes. With increasing the ion density a narrower sheath is needed to shield the wall potential, but due to the fast decline of the ion density near the wall, the absolute wall potential increases slightly.

As the magnetic field intensity approaches the critical value $B_{cr} \simeq 24$ kG, remarkable changes occur in the distributions of the sheath quantities. Contrary to the results of the previous step, the sheath thickness increases with increasing the magnetic field intensity and there appear large inhomogeneities superposed on the usual layered structure of the dusty plasma sheath, which is obvious from the dotted curves in Fig. 2. To understand this behavior, let us discuss the effect of the magnetic field on the spatial distribution of the dust particles. Since the magnetic force tries to decelerate the dust grains, then with increasing the strength of the magnetic field the amplitude of the dust stratification increases. But this aggregation of the dust particles produces an electric field which weakens the sheath electric field at larger ξ. Consequently, the dust stratification is also weekend at larger ξ up to the point where the electric field due to dust aggregation becomes negligible. This process is repeated again to create the next aggregation of the dusts and continues as far as the wall is reached. Although the magnetic field is constant and the magnetic force changes only due to the change in the dust charge, but the electric force becomes very strong as the dusts approach the wall. Therefore, as seen from dotted N_d curves in Fig. 2, the large inhomogeneity is intensified as we move toward the wall. Because of this large inhomogeneity in the dust distribution and the corresponding changes in the ion density, the mean positive charge density decreases along the sheath and to provide an effective shielding the sheath is broadened.

To investigate the dependence of the sheath quantities on the angle of incidence of the magnetic field, Fig. 3 displays the spatial distributions of the electrostatic potential, dust charge, and the normal velocities and number densities of the dusts and plasma particles in the presence of a weak magnetic field with $B=755$ G, for three different values of θ. The sheath thickness and the absolute wall potential decrease as the angle of incidence increases. Since the strength of the z component of the magnetic force increases with increasing θ, then according to Eqs. (32) and (34) this prevents the ions from reaching the wall and accelerates the electrons. Therefore, as seen from the solid and dotted curves in Fig. 3, close to the wall, the ion normal velocity decreases (note that the wall position changes with θ) and the ion number density increases while the reverse is true for the electron normal velocity and its number density, respectively. Therefore, the net electric current flowing onto the wall decreases and this

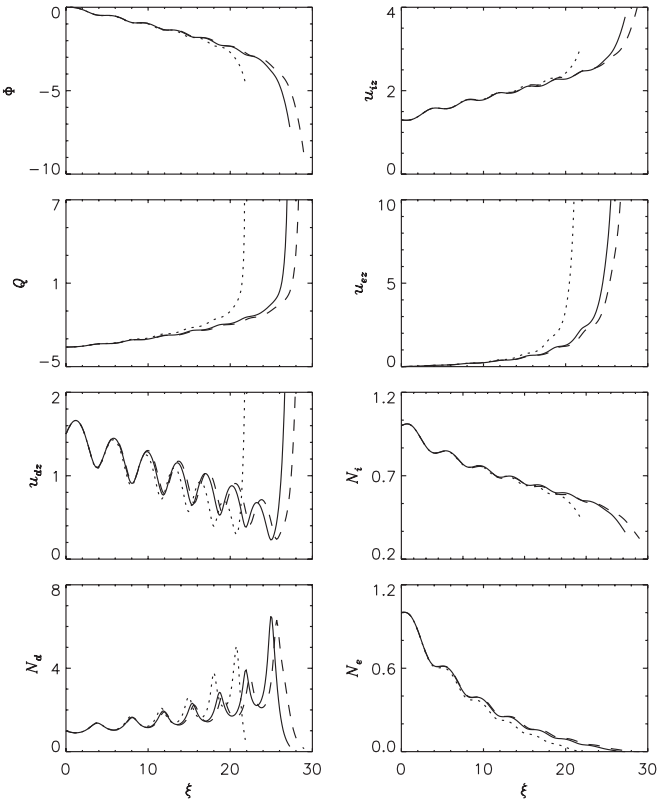

FIG. 3. Effect of the angle of incidence of the magnetic field on the sheath potential, the dust charge, the particle densities, and the particle velocities: $\theta=20°$ (dashed curves), 60° (solid curves), and 80° (dotted curves). The magnetic field intensity is $B=755$ G and all the other parameters are set to their default values.

results in a smaller absolute wall potential. Moreover, in response to the larger ion density and smaller wall potential, the sheath thickness decreases. On the other hand the enhancement of the ion density and reduction in the electron density reduce the net dust charging current, so the absolute value of the dust charge decreases and even changes sign quickly. Figure 3 shows no large inhomogeneity like the one observed in Fig. 2. However, by increasing the strength of the magnetic field to $B=7.5$ kG, the inhomogeneities appear for angles larger than 22° as is obvious from dotted N_d curves in Fig. 4. Then it is concluded that there is a minimum value for $B \sin \theta$ to develop the large inhomogeneity. On the other hand, by comparing the dotted N_d curves from Figs. 2 and 4, we find that the length scale of the inhomogeneity depends on the strength of the magnetic field.

B. Properties of the dust particles

Now we study the effects of changing the dust number density and dust Mach number on the structure of the magnetized dusty plasma sheath. In the usual electron-ion plasma, due to the charge neutrality condition there is a balance between the number of electrons and ions in the bulk plasma. But this is not the case in dusty plasmas. As more electrons attach to the dust particles than the ions, then normally in dusty plasma the ion number density is larger than the electron number density. The ratio of the ion to electron density is determined by the dusts number density and their

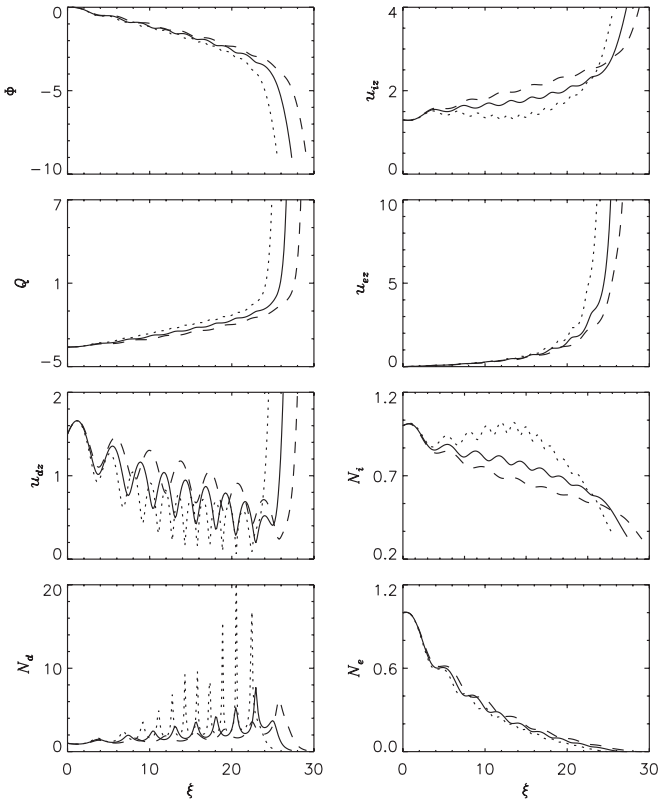

FIG. 4. Same as Fig. 3 except here $B=7.5$ kG and the dashed, solid, and dotted curves are for $\theta=0°$, 22°, and 33°, respectively.

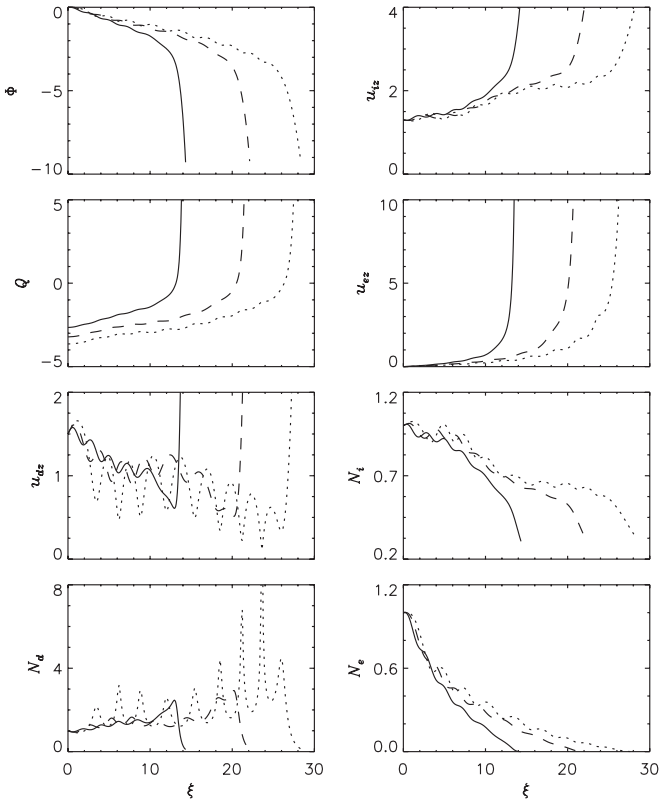

FIG. 5. The distributions of the sheath potential, the dust charge, the particle densities, and the particle velocities for three different values of the ratio of ion-to-electron density at the sheath edge: $\delta^2=1.8$ (dotted curves), 3 (dashed curves), and 6 (solid curves).

radius. For a given dust radius, changing this ratio is equivalent to changing the dust number density or the dust charge. Figure 5 displays the structure of the magnetized dusty plasma sheath for three different values of the ion-to-electron density ratio. The dust particles have the role of sinks for the plasma particles. With increasing the dust number density, more plasma particles, specially much more electrons are collected by the dusts and the ratio of ion-to-electron density increases in the sheath. So, a narrower sheath is needed to shield the wall potential as is obvious from Fig. 5. On the other hand since the electrons are now less populated than the ions the absolute dust charge decreases very strongly. This would be more clear if we note that for the default parameters used in this work we have $q_d/e \simeq 10^3 Q$. Therefore, both the electric and magnetic forces are seriously cut down, and as a result the inhomogeneities on the dust density are almost smoothed out.

In most experimental situations the dust particles are introduced into the plasma by a dust dropper located at the top of the vacuum chamber.[60] The particles fall freely from the rest due to the gravitational force and depending on their height and the bulk plasma parameters enter the sheath with different velocities. So, the dust velocity at the edge of the sheath or equivalently the dust Mach number is a function of the experimental conditions and can be adjusted to a specific value. Figure 6 represents the profiles of the sheath potential, the dust charge, the particles densities, and velocities as functions of ξ for three different values of the dust Mach number. It is clearly seen that changing the dust Mach number has strong effects on the structure of the dusty plasma sheath. The sheath thickness and the dust charge are reduced considerably while the absolute wall potential increases slightly. The large inhomogeneity, specially on the dust distribution, is smoothed out and the small inhomogeneities caused by stratification are broadened. This is because, with increasing the dust Mach number the electrostatic and magnetic forces, which try to decelerate the dust particles, become less effective and the dusts move to the wall quickly. So the dust density increases near the wall and the electrons are then rapidly depleted. The ion density becomes much larger than the electron density and the sheath width decreases. The broadening of the small inhomogeneities in the dust distribution can also be explained similarly.

C. Bulk plasma parameters

Figure 7 shows the effects of changing the bulk plasma electron number density n_{e0} on the structure of the sheath and spatial distributions of the associated quantities. Since δ is kept fixed the situation is identical with changing the bulk plasma number density. It is seen that the sheath thickness increases significantly with increasing the electron number density but the absolute wall potential decreases. The dust charge remains negative even for distances too close to the wall and then changes sign abruptly just before the wall is reached. The number of small as well as large inhomogeneities increases but their amplitude decreases except for situations close to the wall. To explain this behavior, it is noted that with increasing n_{e0} the electron Debye length becomes

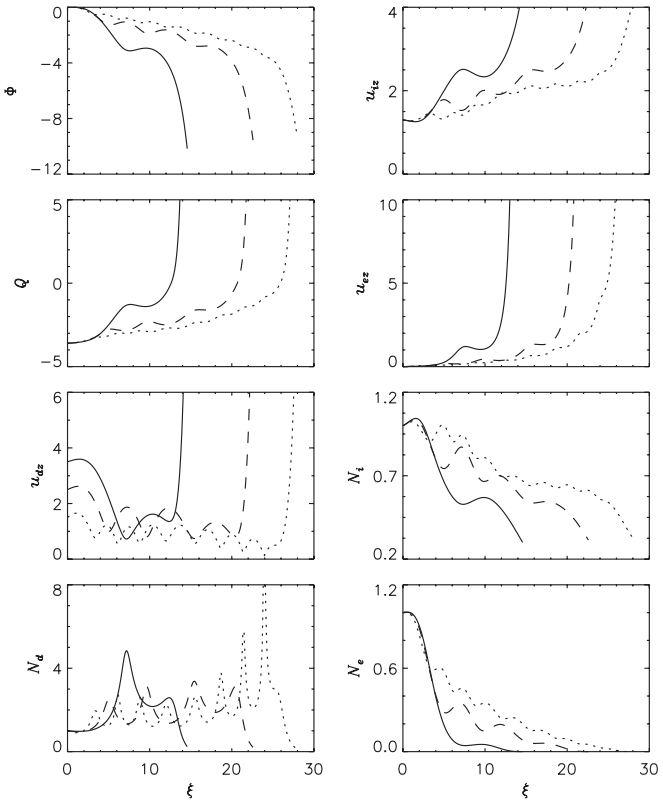

FIG. 6. Profiles of the sheath potential, the dust charge, the particle densities, and the particle velocities as functions of ξ for three different dust Mach numbers: $M_d=1.5$ (dotted curves), 2.5 (dashed curves), and 3.5 (solid curves).

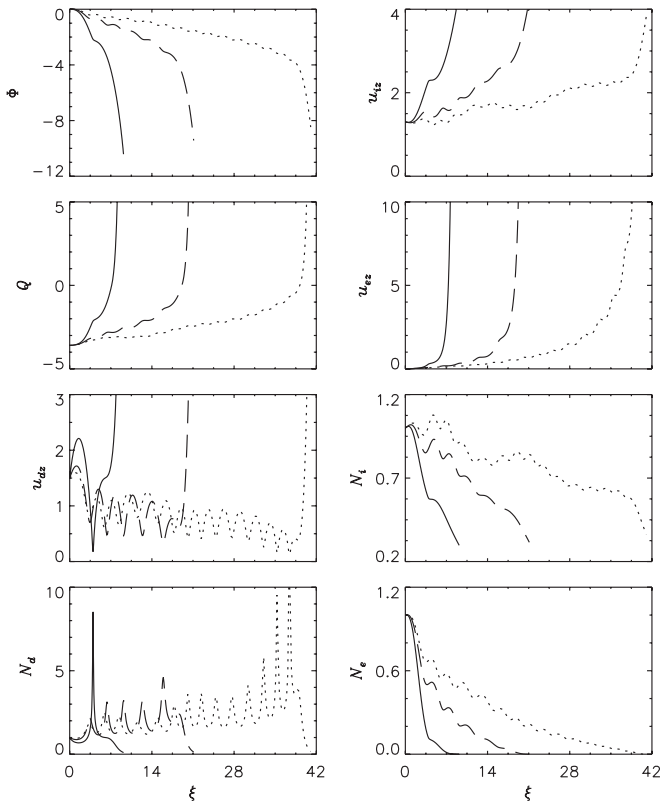

FIG. 7. The profiles of the electrostatic sheath potential, the dust charge, the particle densities, and the particle velocities as functions of ξ for three different values of the electron number density at the sheath edge: $n_{e0}=5\times10^7$ cm^{-3} (solid curves), 5×10^8 cm^{-3} (long-dashed curves), and 2.5×10^9 cm^{-3} (dotted curves). All the other parameters set at their default values.

smaller so the broadening of the sheath is mainly attributed to the change in the length scale, used in the normalization. On the other hand since more electrons attach to the dust particles than the ions, then the number of electrons reaching the wall decreases and the absolute wall potential gets smaller. With more electrons available, the dust charge grows and the decelerating electrostatic and magnetic forces become stronger so the number of inhomogeneities in the dust number density increases.

As the dust charge is mainly determined by the electron current, the electron temperature plays an important role in determining the dynamics of a dusty plasma sheath. In Fig. 8 we have plotted the distributions of the sheath quantities as functions of ξ for three different values of the electron temperature. The system demonstrates a nonlinear behavior. As the electron temperature rises, the sheath thickness first increases and then declines. It is noteworthy that the normalization length scale increases monotonically with increasing the electron temperature. So it cannot be accounted for the observed nonlinearity. To understand the origin of this nonlinearity we examine the temperature dependence of the electron density and the charging current of the dusts. Neglecting the magnetic and collisional forces, the electron distribution can be approximated by the Boltzmann factor $\exp(e\phi/T_e)$. On the other hand the electron current flowing onto the dust grains is proportional to $T_e^{1/2}\exp(eq_d/r_dT_e)$. By comparing the magnitudes of Q and Φ in Fig. 8 and remembering the way they were made dimensionless by using Eq. (24), we find that the dust charging current is more sensitive to the variation in the electron temperature than the Boltzmann factor. However, the later has a direct impact on the dynamics of the sheath by changing the electron number density, while the former has an implicit and more complicated role in the formation and properties of the sheath. The electrons collected by the dust particles never totally removed from the sheath because they are still on the dust particles but their influence is significantly reduced, since the dust charge is determined by both of the electron and ion currents. Therefore, with rising the electron temperature the sheath first is broadened due to the increase in the electron density, as a thicker positive column is needed to protect the bulk plasma from the electric field. But then at much higher electron temperature the dust charging factor becomes dominant and reduces the electron density substantially. So an almost pure ion sheath is left and the sheath width decreases. From Eq. (29) it is inferred that the ion density is affected by the variation in the electron temperature and electron number density. To provide the Debye shielding the ion density should increase with the enhancement of the electron density and vice versa. Then with growing the electron temperature the absolute wall potential first decreases and then increases, respectively. Likewise, the variation in the width and amplitude of

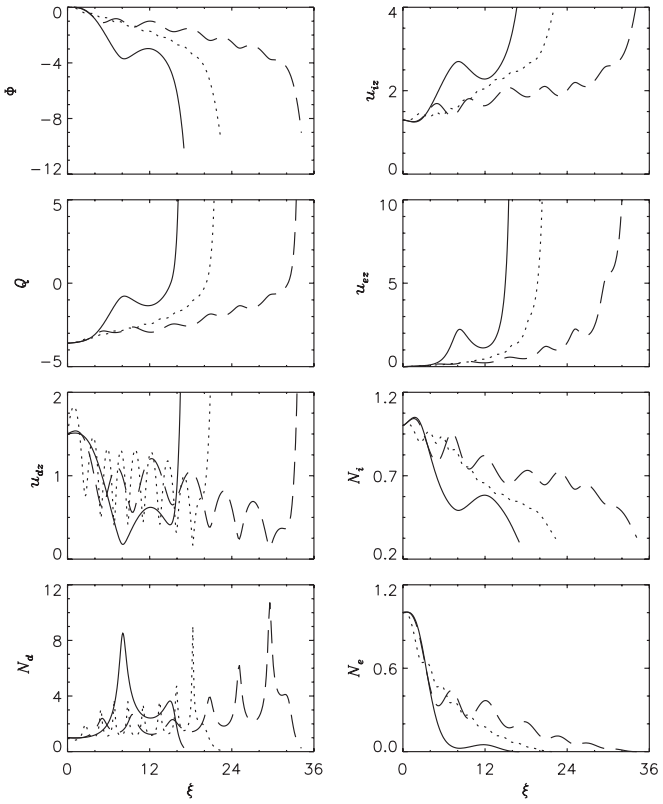

FIG. 8. Effect of variation in the electron temperature on the spatial distributions of the sheath potential, the dust charge, the particle densities, and the particle velocities: T_e=0.5 eV (dotted curves), 3 eV (long-dashed curves), and 7 eV (solid curves). All the other parameters are set to their default values.

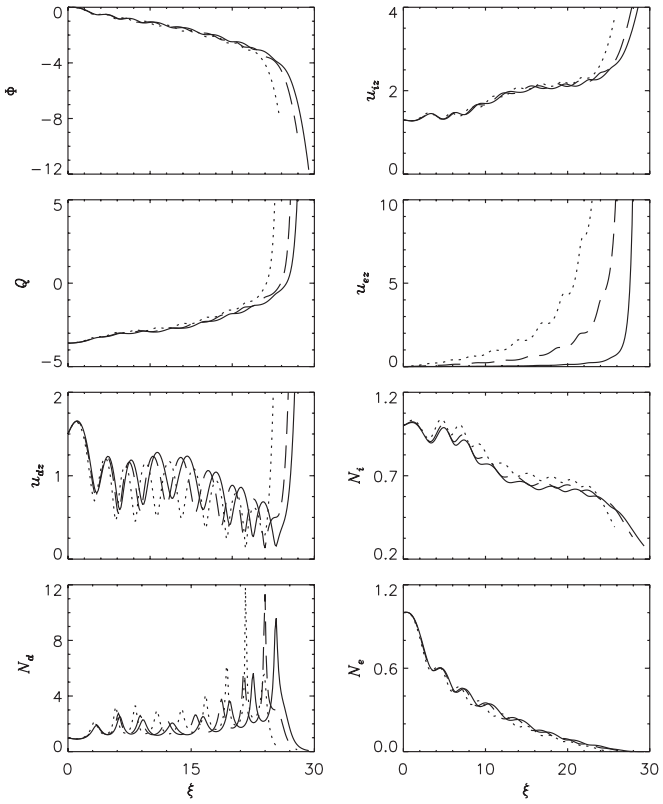

FIG. 9. The results of the numerical simulations for distributions of the sheath potential, the dust charge, the particle densities, and the particle velocities for three different values of the ionization frequency: ν_{ion}=0.001 (solid curves), 0.01 (long-dashed curves), and 0.03 (dotted curves).

the density fluctuations in the dust distribution can be explained in terms of the change in the strength of the electric field and magnitude of the dust charge.

Finally, we study the effect of changing the ionization frequency on the dynamics of the sheath and the spatial distributions of the relevant quantities. Figure 9 displays the structure of the sheath for three different ionization frequencies. With increasing the ionization frequency more electrons and ions are produced, and we expect that their number densities both would be increased. But this is not the case for the electrons because they are effectively collected by the dust particles. Thus as seen from Fig. 9 the electron number density remains intact while the ion density increases. Because of this, the absolute wall potential decreases and the sheath becomes narrower. Since the dust particles gain more electrons, the decelerating electric and magnetic forces are intensified and the amplitude of the fluctuations in the dust distribution increases.

IV. SUMMARY AND CONCLUSIONS

In this work, using numerical simulations of the multifluid equations, we have studied the structure of a dusty plasma sheath in an external oblique magnetic field. We have investigated the impacts of the different parameters of the magnetic field, the dust particles, and the bulk plasma on the spatial distributions of the electrostatic potential, the dust charge, and the normal velocity and number density of the dust grains, ions, and electrons. The main results of this work are as follows.

(i) With increasing the intensity of the magnetic field from 0 to moderate values (e.g., 7.5 kG), the sheath thickness, the absolute dust charge, the electron number density, and the normal velocities of the ions and dust particles decrease while the ion number density, the absolute wall potential, and the level of stratification in the dust distribution increase. This can be explained in terms of the magnetic force on the particles which decelerates the normal motion of the ions and dust particles but accelerates the electrons. When the magnetic field intensity is further increased to magnitudes close to the critical value of $\simeq$24 kG, the sheath is broadened and regular large inhomogeneities develop on the small density stratification of an electrostatic dusty plasma sheath. This can be attributed to the creation of large scale electric gradients due to aggregation of the dust particles which affects the spatial distribution of the dusts, and somewhat weaker the other sheath parameters.

(ii) At a given magnetic field intensity, increasing the angle of incidence of the magnetic field leads to the reduction in the sheath thickness and the absolute values of the wall potential and the dust charge. The large density inhomogeneities do not appear for weak magnetic fields and also at small angles of incidence.

It seems that there is a minimum value for $B \sin \theta$ to develop the large inhomogeneities.[56,57]

(iii) When the dust number density increases, the loss of the plasma particles due to attachment to the dust grains increases, and since the dust particles collect more electrons than the ions, the electron density declines rapidly. Then the sheath thickness and the absolute dust charge are strongly reduced, and due to weak electric and magnetic forces the inhomogeneities in the dust distribution are smoothed out.

(iv) Changing the dust Mach number has also strong impacts on the structure of the sheath. The sheath thickness and absolute dust charge are effectively reduced and the large inhomogeneities are smoothed out while the small inhomogeneities are broadened.

(v) As the number density of the bulk plasma increases, the absolute wall potential decreases but the absolute dust charge increases. Then the electric and magnetic forces become stronger and the numbers of both large and small inhomogeneities increase but their amplitudes decline. The change in the sheath width is mainly due to the change in the electron Debye length used in the normalization.

(vi) The system shows a nonlinear behavior against the variation in the electron temperature. As the electron temperature rises, the sheath thickness first increases and then declines. This is due to competition between the two effects of increasing the electron number density through the Boltzmann factor and decreasing it via the collection of the electrons by the dust particles. At moderate temperatures the first effect prevails and the electron density increases. But at higher temperatures the second one becomes dominant and the electron density decreases. Consequently, to provide an effective shielding, the sheath is broadened first and the ion density increases near the wall so the absolute wall potential decreases, but then the sheath becomes narrower and the ion density decreases and because of that the absolute wall potential increases.

(vii) The electrons are collected by the dust particles more efficiently than the ions. Therefore, with increasing the ionization frequency the electron number density remains almost unchanged but the absolute dust charge and the ion number density increase. Then the absolute wall potential and the sheath thickness decrease while the level of fluctuation in the dust number density increases.

The above numerical results yield an improved understanding of the dynamics and structure of the dusty plasma sheath in an oblique magnetic field. The results obtained in this work are of practical importance in a wide range of industrial applications specially in plasma-aided material processing and plasma-aided nanofabrication. Extension of the present results and their application to study the growth and properties of different plasma-produced nanostructures and comparison between the simulations and existing experimental findings would be highly valuable and are left for future works.

ACKNOWLEDGMENTS

We wish to thank Professor P. A. Robinson for his helpful comments. This work was supported by Sahand University of Technology.

[1] M. A. Lieberman and A. J. Lichtenberg, *Principles of Plasma Discharges and Materials Processing* (Wiley, New York, 1994).
[2] P. C. Stangeby, *The Plasma Boundary of Magnetic Fusion Devices* (IOP, Bristol, 2000).
[3] I. H. Hutchinson, *Principles of Plasma Diagnostics*, 2nd ed. (Cambridge University Press, Cambridge, 2002).
[4] V. A. Godyak and N. Sternberg, IEEE Trans. Plasma Sci. **18**, 159 (1990).
[5] K.-U. Riemann, J. Phys. D **24**, 493 (1991).
[6] T. E. Sheridan and J. Goree, Phys. Fluids B **3**, 2796 (1991).
[7] H.-B. Valentini, Phys. Plasmas **3**, 1459 (1996).
[8] X. P. Chen, Phys. Plasmas **5**, 804 (1998).
[9] R. N. Franklin, J. Phys. D **36**, R309 (2003).
[10] K.-U. Riemann, J. Phys. D **36**, 2811 (2003).
[11] B. Alterkop, J. Appl. Phys. **95**, 1650 (2004).
[12] K.-U. Riemann, Phys. Plasmas **13**, 063508 (2006).
[13] R. Chodura, Phys. Fluids **25**, 1628 (1982).
[14] G. H. Kim, N. Hershkowitz, D. A. Diebold, and M.-H. Cho, Phys. Plasmas **2**, 3222 (1995).
[15] K.-U. Riemann, Phys. Plasmas **1**, 552 (1994).
[16] I. H. Hutchinson, Phys. Plasmas **3**, 6 (1996).
[17] P. C. Stangeby, Phys. Plasmas **2**, 702 (1995).
[18] H. Schmitz, K. U. Riemann, and Th. Daube, Phys. Plasmas **3**, 2486 (1996).
[19] Th. Daube, K.-U. Riemann, and H. Schmitz, Phys. Plasmas **5**, 117 (1998).
[20] Th. Daube and K.-U. Riemann, Phys. Plasmas **6**, 2409 (1999).
[21] R. N. Franklin and J. Snell, J. Phys. D **32**, 1031 (1999).
[22] D. Sharma and H. Ramachandran, J. Nucl. Mater. **290–293**, 725 (2001).
[23] F. Valsaque and G. Manfredi, J. Nucl. Mater. **290–293**, 763 (2001).
[24] D. Sharma and H. Ramachandran, Phys. Rev. E **66**, 026412 (2002).
[25] D. Tskhakaya and S. Kuhn, J. Nucl. Mater. **313–316**, 1119 (2003).
[26] N. Sternberg and J. Poggie, IEEE Trans. Plasma Sci. **32**, 2217 (2004).
[27] X. Zou, J.-Y. Liu, Y. Gong, Z.-X. Wang, Y. Liu, and X.-G. Wang, Vacuum **73**, 681 (2004).
[28] R. N. Franklin, J. Phys. D **38**, 3412 (2005).
[29] D. D. Tskhakaya, P. K. Shukla, B. Eliasson, and S. Kuhn, Phys. Plasmas **12**, 103503 (2005).
[30] E. C. Whipple, Rep. Prog. Phys. **44**, 1198 (1981).
[31] E. C. Whipple, T. G. Northrop, and D. A. Mendis, J. Geophys. Res. **90**, 7405, doi:10.1029/JA090iA08p07405 (1985).
[32] T. G. Northrop, D. A. Mendis, and L. Schaffer, Icarus **79**, 101 (1989).
[33] A. V. Gurevich and L. P. Pitaevsky, Prog. Aerosp. Sci. **16**, 227 (1975).
[34] C. K. Goertz, Rev. Geophys. **27**, 271, doi:10.1029/RG027i002p00271 (1989).
[35] T. G. Northrop, Phys. Scr. **45**, 475 (1992).
[36] S. Robertson, Phys. Plasmas **2**, 2200 (1995).
[37] B. Walch, M. Horanyi, and S. Robertson, Phys. Rev. Lett. **75**, 838 (1995).
[38] N. N. Rao, P. K. Shukla, and M. Y. Yu, Planet. Space Sci. **38**, 543 (1990).
[39] R. K. Varma, P. K. Shukla, and V. Krishan, Phys. Rev. E **47**, 3612 (1993).
[40] M. R. Jana, A. Sen, and P. K. Kaw, Phys. Rev. E **48**, 3930 (1993).
[41] S. V. Vladimirov, Phys. Rev. E **49**, R997 (1994); Phys. Plasmas **1**, 2762 (1994).
[42] G. S. Selwyn, J. E. Heidenreich, and K. L. Haller, Appl. Phys. Lett. **57**, 1876 (1990).
[43] B. Lipschultz, J. Nucl. Mater. **145–147**, 15 (1987).
[44] M. Y. Yu, H. Saleem, and H. Luo, Phys. Fluids B **4**, 3427 (1992).
[45] D. Winske and M. E. Jones, IEEE Trans. Plasma Sci. **22**, 454 (1994).
[46] J. X. Ma and M. Y. Yu, Phys. Plasmas **2**, 1343 (1995).
[47] T. Nitter, Plasma Sources Sci. Technol. **5**, 93 (1996).
[48] J. X. Ma, J.-y. Liu, and M. Y. Yu, Phys. Rev. E **55**, 4627 (1997).
[49] V. N. Tsytovich, S. V. Vladimirov, and S. Benkadda, Phys. Plasmas **6**, 2972 (1999).
[50] M. K. Mahanta and K. S. Goswami, Phys. Plasmas **8**, 665 (2001).
[51] S. Takamura, T. Misawa, N. Ohno, S. Nunomura, M. Sawai, K. Asano, and P. K. Kaw, Phys. Plasmas **8**, 1886 (2001).

[52]G. Sorasio, D. P. Resendes, and P. K. Shukla, JETP Lett. **74**, 77 (2001).
[53]D. P. Resendes, G. Sorasio, and P. K. Shukla, Phys. Plasmas **9**, 2988 (2002).
[54]S. K. Baishya and G. C. Das, Phys. Plasmas **10**, 3733 (2003).
[55]J.-Y. Liu, Z.-X. Wang, X. Wang, Q. Zhang, X. Zou, and Y. Zhang, Phys. Plasmas **10**, 3507 (2003).
[56]G. C. Das and P. Kalita, J. Phys. D **37**, 702 (2004).
[57]M. Davoudabadi and F. Mashayek, Phys. Plasmas **12**, 073505 (2005).
[58]M. Davoudabadi, B. Rovagnati, and F. Mashayek, IEEE Trans. Plasma Sci. **34**, 142 (2006).
[59]B. P. Pandey, A. Samarian, and S. V. Vladimirov, Phys. Plasmas **14**, 093703 (2007).
[60]N. C. Adhikary, H. Bailung, A. R. Pal, J. Chutia, and Y. Nakamura, Phys. Plasmas **14**, 103705 (2007).
[61]A. Barkan, R. L. Merlino, and N. D'Angelo, Phys. Plasmas **2**, 3563 (1995).
[62]P. K. Shukla and A. A. Mamun, *Introduction to Dusty Plasma Physics* (IOP, Bristol, 2002).
[63]V. N. Tsytovich, N. Sato, and G. E. Morfill, New J. Phys. **5**, 43 (2003).
[64]M. S. Barnes, J. H. Keller, J. C. Forster, J. A. O'Neill, and D. K. Coultas, Phys. Rev. Lett. **68**, 313 (1992).
[65]D.-Z. Wang and J. Q. Dong, J. Appl. Phys. **81**, 38 (1997).